

**Gold nanoparticles as markers for fluorinated surfaces  
containing embedded amide groups**

Barbara Ballarin<sup>a,\*</sup>, Davide Barreca<sup>b</sup>, Maurizio Bertola<sup>c</sup>, Maria Cristina Cassani<sup>a,\*</sup>,

Giorgio Carraro<sup>d</sup>, Chiara Maccato<sup>d</sup>, Adriana Mignani<sup>a</sup>,

Daniele Nanni<sup>a</sup>, Chiara Parise<sup>a</sup>, Silvia Ranieri<sup>a</sup>

*<sup>a</sup> Department of Industrial Chemistry “Toso Montanari”, UdR INSTM of Bologna, Alma Mater Studiorum – Bologna University and INSTM, Viale del Risorgimento 4, I-40136-Bologna, Italy*

*<sup>b</sup> CNR-ICMATE and INSTM, Department of Chemical Sciences, Padova University, Via Marzolo 1, I-35131 Padova, Italy*

*<sup>c</sup> Miteni S.p.A., Località Colombara 91, I-36070 Trissino (VI), Italy*

*<sup>d</sup> Department of Chemical Sciences, Padova University and INSTM, Via Marzolo 1, I-35131 Padova, Italy*

\* Corresponding authors. barbara.ballarin@unibo.it; Fax: +39 0512093694; Phone: +39 0512093704 (B.B.); maria.cassani@unibo.it; Fax: +39 0512093694; Phone: +39 0512093700.

## Abstract

Indium tin oxide (ITO) substrates were functionalized with fluoroalkylsilanes (FAS) having formula  $R_F C(O)N(R)(CH_2)_3Si(OMe)_3$  (**1**,  $R = H$ ,  $R_F = C_5F_{11}$ ; **2**,  $R = CH_3$ ,  $R_F = C_5F_{11}$ ; **3**,  $R = H$ ,  $R_F = C_3F_7$ ) and containing embedded amide moieties between the perfluoroalkyl chain and the syloxanic moiety. Subsequently, Au nanoparticle deposition ( $Au_{NPs}$ ) onto the ITO-FAS functionalized surfaces was carried out by immersion into a solution of citrate-stabilized  $Au_{NPs}$ . The ITO-FAS and  $Au_{NPs}$ /ITO-FAS modified systems were characterized by various complementary techniques and compared with  $Au_{NPs}$ /ITO modified with  $R_F(CH_2)_2Si(OEt)_3$  (**4**,  $R_F = C_6F_{13}$ ), free from functional groups between the fluorinated tail and the syloxanic moiety. The results showed that only ITO glasses modified with **1**, **2** and **3** displayed an oleophobic, as well as hydrophobic, behaviour and that the  $Au_{NPs}$  Surface Coverage (SC %) directly depended on the fluoroalkylsilane nature with the following trend: 60% **ITO-2** > 16% **ITO-3** > 9% **ITO-1** > 3% **ITO-4**. The obtained results revealed that, in organosilane **2**, the presence of a methyl group on the amide nitrogen increases the steric hindrance in the rotation around the *N*-CO bond, resulting in the co-presence of two stable conformers in comparable amounts. Their co-presence in solution, combined with the lack of intermolecular *N*-H...OC-*N* hydrogen bonds among the anchored molecules, has dramatic influences on the functionalized ITO, yielding a disorderedly packed coating able to accommodate a large quantity of  $Au_{NPs}$ . These results indicate that  $Au_{NPs}$  can act as excellent probes to evaluate the coating layer quality but, at the same time, it is possible to tune the gold loading on electroactive surfaces depending on the chemical structure of the used fluorinated silane.

**Keywords:** indium tin oxide; environmentally safer fluoroalkylsilanes; amide groups; amide rotational barrier; gold nanoparticles; surface coverage.

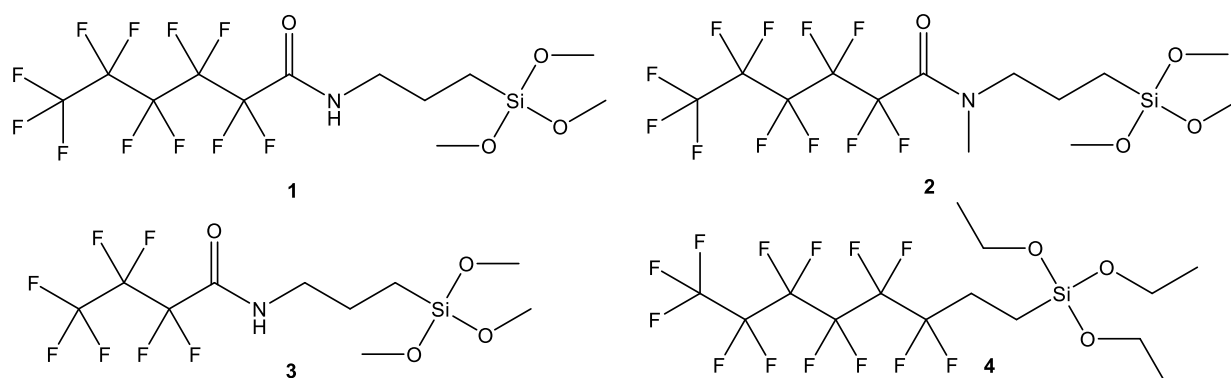
## 1. Introduction

Fluorinated thin films serve as vital tools for the fabrication of functional surfaces, such as coinage metals for corrosion prevention, inorganic oxides for self-cleaning [1][2][3], steel or electronic devices as anti-fouling and anti-fingerprint coatings [4][5][6][7]. The increasing concern on long perfluorinated alkyl chains owing to their bioaccumulation, toxicity and environmental persistence has boosted the attention on environmentally safer building blocks with short perfluorinated carbon chains, involving no more than six carbon atoms [8][9][10]. Nevertheless, in spite of the lower impact on the environment and human health, the latter systems display worse performances in applications where a large content of fluorine atoms is mandatory in order to achieve a significant oleo- and hydrophobicity. As a consequence, advanced synthetic strategies in this field cannot simply involve shortening of the fluorocarbon chain, but have also to include a complete molecule re-design, in order to simultaneously meet all the pending requirements. Once the task of producing new and safer FAS is accomplished, the investigation of their arrangement on different surfaces is of great importance, and gold nanoparticles  $Au_{NPs}$  has proved to be excellent probes for the evaluation even of small variations in the coating layer structure [11][12][13][14].

Within this frame, recently we have investigated the properties of indium tin oxide electrodes (ITO) modified with environmentally safer fluoroalkylsilanes (FAS, perfluorinated alkyl chain  $R_F < 6$  carbon atoms) through the chemisorption of FAS molecules onto the surface bound silanols [15]. We found that in the organosilane  $C_5F_{11}C(O)N(H)(CH_2)_3Si(OMe)_3$  (**1** in Scheme 1) the embedded amide group, promoting intermolecular hydrogen bonding among the anchored molecules [16][17], plays an important role and can balance the lower fluorine content. Indeed, the surface of ITO modified with **1** (**ITO-1**) presents a contact angle (CA) and a surface energy similar to FAS with  $R_F > 6$  and typical of amphiphobic materials. Subsequently, we have investigated and compared the properties of citrate-stabilized  $Au_{NPs}$  deposited on **ITO-1** with those obtained by depositing  $Au_{NPs}$  on bare ITO and on an ITO previously silanized with  $C_6F_{13}(CH_2)_2Si(OEt)_3$  (**4**, in Scheme 1), free from functional groups between the fluorinated tail and the syloxanic moiety [18]. A combination of

spectroscopic and electrochemical characterization was used to attain a thorough insight into the influence of the amide functional group on the system morphology and electrocatalytic behaviour.

Encouraged by our previous results, in the present investigation we have further investigated the influence of an embedded amide moiety on the structure and orientation of these type of molecules bound to the surface, and examined the effect of a further reduction of the fluorinated tail length. To accomplish these goals, the new organosilanes **2** and **3** depicted in Scheme 1 have been employed.



**Scheme 1.** Chemical structure of the monomers used for the ITO modification.

Compound **2** differs from **1** by the presence of a methyl group on the amide nitrogen, whereas in **3** the perfluorinated tail is two  $\text{CF}_2$  units shorter. The methyl group on the amide nitrogen in **2** plays a twofold role: i) it acts as a probe to study the role of hydrogen bonding on the morphology of the coating layer; ii) it affects the rotational barrier around the  $N\text{-CO}$  bond, giving rise to two different  $E/Z$  conformers that can eventually impact the packing of the anchored FAS molecules.

The modified ITO glasses have been subsequently treated with  $\text{AuNPs}$ , and the  $\text{AuNPs}/\text{FAS}$ -ITO structures were characterized by different techniques to study the interplay between the molecular structure of the FAS molecules and the properties of the produced materials.

## 2. Experimental

### 2.1. Materials and procedures

The chemicals 3,3,4,4,5,5,6,6,7,7,8,8,8-tridecafluorooctyltriethoxysilane (**4**), diiodomethane,  $K_3[Fe(CN)_6]$ ,  $K_4[Fe(CN)_6]$ ,  $KNO_3$ , sodium citrate ( $Na_3C_6H_5O_7$ ) were purchased from Sigma-Aldrich<sup>®</sup> and used without any purification. Ultrapure water purified by the Milli-Q plus system (Millipore Co., resistivity over 18 M $\Omega$ cm) was used in all cases. The organosilanes **1**, **2**, **3** were prepared in-house by Miteni S.p.A. [19] *via* Electrochemical Fluorination (ECF) [20][21] and the NMR and IR-ATR characterization for **2** and **3** are reported below. All the organosilanes are stored under nitrogen prior to use.

NMR and IR-ATR characterization for **2** (*vide infra* for the Variable Temperature NMR characterization).  $^1H$ -NMR (399.9 MHz,  $CDCl_3$ , 298 K)  $\delta$ : 3.56 (s, 9H,  $Si(OCH_3)_3$ ), 3.41 (t,  $^3J_{H,H} = 8.0$  Hz, 2H,  $NCH_2CH_2CH_2Si^-$ ), 3.12, 3.01 (s, 3H,  $NCH_3$ ), 1.68 (m, 2H,  $NCH_2CH_2CH_2Si^-$ ), 0.58 (m, 2H,  $NCH_2CH_2CH_2Si^-$ ).  $^{13}C$ -NMR (100.6 MHz,  $CDCl_3$ , 298 K)  $\delta$ : 157.4 (t,  $^2J_{C,F} = 34$  Hz, CO), 120.0–105.0 (m,  $C_3F_{11}$ ), 52.5 ( $NCH_2CH_2CH_2Si^-$ ), 50.5 ( $SiOCH_3$ ), 35.2 ( $NCH_3$ ), 19.7 ( $NCH_2CH_2CH_2Si^-$ ), 6.1 ( $NCH_2CH_2CH_2Si^-$ ).  $^{19}F$ -NMR (375.9 MHz,  $CDCl_3$ , 298 K)  $\delta$ : -80.8 ( $CF_3$ ), -111.7 ( $CF_2$ ), -121.2 ( $CF_2$ ), -121.5 ( $CF_2$ ), -126.4 ( $CF_2$ ). IR-ATR (neat liquid,  $cm^{-1}$ ): 2948, 2845 (m,  $\nu$ CH), 1683 (s,  $\nu$ CO), 1080–1200 (vs,  $\nu$ SiO and  $\nu$ CF overlapping bands), 814 (s,  $\nu$ CF).

NMR and IR-ATR characterization for **3**.  $^1H$  NMR (399.9 MHz,  $CDCl_3$ , 298 K)  $\delta$ : 7.20 (bs, 1H, NH), 3.36 (m, 2H,  $NCH_2CH_2CH_2Si^-$ ), 1.70 (m, 2H,  $NCH_2CH_2CH_2Si^-$ ), 0.65 (m, 2H,  $NCH_2CH_2CH_2Si^-$ ).  $^{13}C$  NMR (100.6 MHz,  $CDCl_3$ , 298 K)  $\delta$ : 157.5(t,  $^2J_{C,F} = 26$  Hz, CO), 120.0–104.0 (m,  $C_3F_7$ ), 50.5 ( $SiOCH_3$ ), 42.2 ( $NCH_2CH_2CH_2Si^-$ ), 21.8 ( $NCH_2CH_2CH_2Si^-$ ), 6.3 ( $NCH_2CH_2CH_2Si^-$ ).  $^{19}F$  NMR (375.9 MHz,  $CDCl_3$ , 298 K)  $\delta$ : -80.8 ( $CF_3$ ), -121.0 ( $CF_2$ ), -127.3 (m,  $CF_2$ ). IR-ATR (neat liquid,  $cm^{-1}$ ): 3319 (m,  $\nu$ NH), 2947, 2845 (m,  $\nu$ CH), 1703 (s,  $\nu$ CO), 1544 (m,  $\delta$ NH), 1080–1200 (vs,  $\nu$ SiO and  $\nu$ CF overlapping bands), 814 (s,  $\nu$ CF).

## 2.2 Sample Preparation

Prior to functionalization, ITO glass slides (Optical Filters Ltd., UK; surface resistivity = 12  $\Omega \times cm$ ;

size = 0.7 cm × 2 cm) were treated in warm acetone for 5 min, rinsed in 1:1 Milli-Q water/isopropanol under sonication for 30 min, washed with Milli-Q water and dried under a N<sub>2</sub> flow [22][23]. Subsequently, the slides were immersed into a 5% (v/v) isopropanol solution of the target fluoroalkylsilane (5 mL) for 24 h under nitrogen at room temperature. The functionalized ITO substrates were thoroughly rinsed with pure isopropanol, dried at 50°C for 2 h and stored under vacuum for 5 h. The FAS were instead recovered for further reuse from the solution removing the isopropanol under vacuum. The obtained ITO-FAS systems were placed in vials containing 5 mL of freshly prepared-citrate stabilized AuNPs [particle size = (14±4) nm] solution for 30 min [18][24], rinsed with MilliQ water, dried and stored under nitrogen. All samples were prepared in triplicate to ensure outcome reproducibility.

### 2.3 Instrumentation

NMR spectra were recorded using Varian Inova 300 (<sup>1</sup>H, 300.1; <sup>13</sup>C, 75.5 MHz), Varian MercuryPlus VX 400 (<sup>1</sup>H, 399.9; <sup>13</sup>C, 100.6 MHz), Varian Inova 600 (<sup>1</sup>H, 599.7; <sup>13</sup>C, 150.8 MHz) instruments. Spectra were internally referenced to residual solvent resonances, and unless otherwise stated, they were recorded at 298 K for characterization purposes; full <sup>1</sup>H and <sup>13</sup>C NMR assignments were done, when necessary, by gCOSY, gHSQC, gHMBC experiments using standard Varian pulse sequences; J.Young valve NMR tubes (Wilmad) were used to carry out NMR experiments under inert conditions. Variable temperature NMR spectra were recorded using spectrometers at 400 and 600 MHz for <sup>1</sup>H in C<sub>2</sub>D<sub>2</sub>Cl<sub>4</sub>. Further details are provided in the Supplementary Information.

DFT Calculations were performed by Molecular Mechanics (MMFF force field as implemented in Titan 1.0.5, Wavefunction Inc.). Final geometry optimizations were carried out at the B3LYP/6-31G(d) level [25] by means of the Gaussian 09 series programs [26]. The standard Berny algorithm in redundant internal coordinates and default criteria of convergence were employed in all calculations. Harmonic vibrational frequencies were calculated for all the stationary points. For each optimized ground state, the frequency analysis showed the absence of imaginary frequencies, whereas

each transition state showed a single imaginary frequency. Visual inspection of the corresponding normal mode was used to confirm the identification of the correct transition state. All the reported energy values, representing total electronic energies, yield the best fit with experimental NMR data [27]. Therefore, the computed numbers have not been corrected for zero-point energy contributions or other thermodynamic parameters. This enables to avoid artifacts that might result from the ambiguous choice of an adequate reference temperature, from the empirical scaling [28], and from the treatment of low-frequency vibration as harmonic oscillators [29].

Further details are provided in the Supplementary Material.

ATR-FT-IR analysis was performed using a Perkin Elmer Spectrum Two spectrophotometer, equipped with an Universal ATR accessory, in the range 4000-400  $\text{cm}^{-1}$  with a resolution of 0.5  $\text{cm}^{-1}$ .

X-ray photoelectron spectroscopy (XPS) investigation was carried out by a Perkin Elmer  $\Phi$  5600ci spectrometer (working pressure  $< 10^{-8}$  mbar), equipped with a standard  $\text{AlK}\alpha$  X-ray source ( $h\nu = 1486.6$  eV). Adventitious C1s peak [Binding Energy (BE) = 284.8 eV] was used for charging correction [30]. The BE standard deviation was estimated to be  $\pm 0.2$  eV. Raw spectra were fitted by means of a non-linear least-squares deconvolution program (Shirley-type background, Gaussian-Lorentzian peak shapes).  $\Phi$  V5.4A sensitivity factors were used for the calculation of atomic percentages (at. %).

Field emission-scanning electron microscopy (FE-SEM) measurements were performed using a Zeiss SUPRA 40VP instrument, using a primary beam acceleration voltage of 10 kV and collecting micrographs with an InLens detector. The ImageJ<sup>®</sup> (<http://imagej.nih.gov/ij/>, accessed July 2017) picture analyzer software was used to estimate the average nanoparticle dimensions and the  $\text{Au}_{\text{NPs}}$  surface coverage ( $\text{Au}_{\text{NPs}}$  SC %). Particle size estimation for each specimen was performed by averaging over various independent measurements.

Electrochemical impedance spectroscopy (EIS) were recorded using a  $\mu$ AUTOLAB type III controlled by a personal computer *via* NOVA 1.6 software, recording data between 10 mHz and 100

KHz. All the electrochemical measurements were conducted in a conventional three-electrode cell using a 0.1 M KNO<sub>3</sub> solution containing 1 mM K<sub>3</sub>[Fe(CN)<sub>6</sub>]/K<sub>4</sub>[Fe(CN)<sub>6</sub>] (1:1) mixture, a SCE reference electrode and a Pt wire counter electrode in a N<sub>2</sub> atmosphere at room temperature. EIS conditions: E<sub>appl</sub> = +0.22 V vs. SCE; each measurement was repeated three times. The standard Randle's equivalent circuit model was used to fit impedance data and to calculate electron transfer resistance (*R<sub>ct</sub>*) and capacitive elements. All the capacitive elements of the equivalent circuit have been substituted with CPE, namely, the "capacitance dispersion" expressed in terms of a constant phase element;  $\chi^2$  values of ca. 6  $\cdot 10^{-5}$  for all fitting results were calculated, yielding an excellent correlation between the experimental and simulated data.

Contact angle (CA) measurements were performed under ambient conditions with a GBX Digidrop Contact Angle Meter, using the sessile drop method. Typically, 1  $\mu$ L water droplets were used for the measurements, and CA values were determined averaging over three measurements. Drop images were recorded with a CCD-camera, after adjusting contrast, magnification and focus.

Surface free energies for all samples and their disperse and polar components were calculated according to the Owens-Wendt-Rabel and Kaelble theory (OWRK method), using water and diiodomethane as standard testing liquids [31].

### 3. Results and Discussion

#### 3.1 Solution NMR Studies

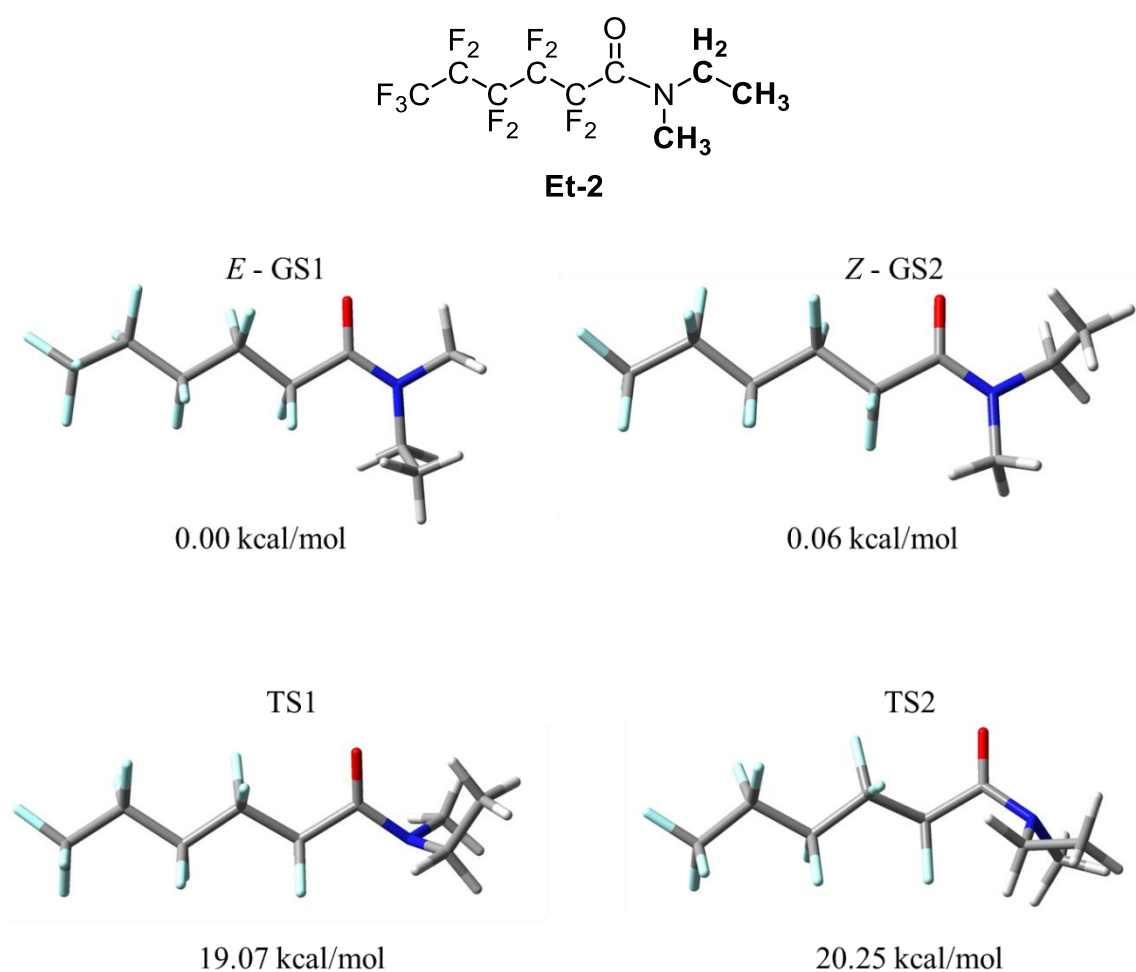
Fluoroalkylsilane **2** (Scheme 1) bears a tertiary amide group, where the *N* is substituted with a methyl and the alkyl silane moieties. From a conformational point of view, amides have been extensively studied [32][33][34] due to the *N*-CO partial double bond character, increasing the rotational barrier about this bond [35][36].

In compound **2**, the long fluorinated chain exerts a strong electron withdrawing effect, enhancing the partial *N*-CO double bond character [37][38][39]. In addition, the methyl group on the



*N* increases the steric hindrance to the rotation, freezing the rotation about *N*-CO bond in the NMR timescale and generating a conformation pairs.

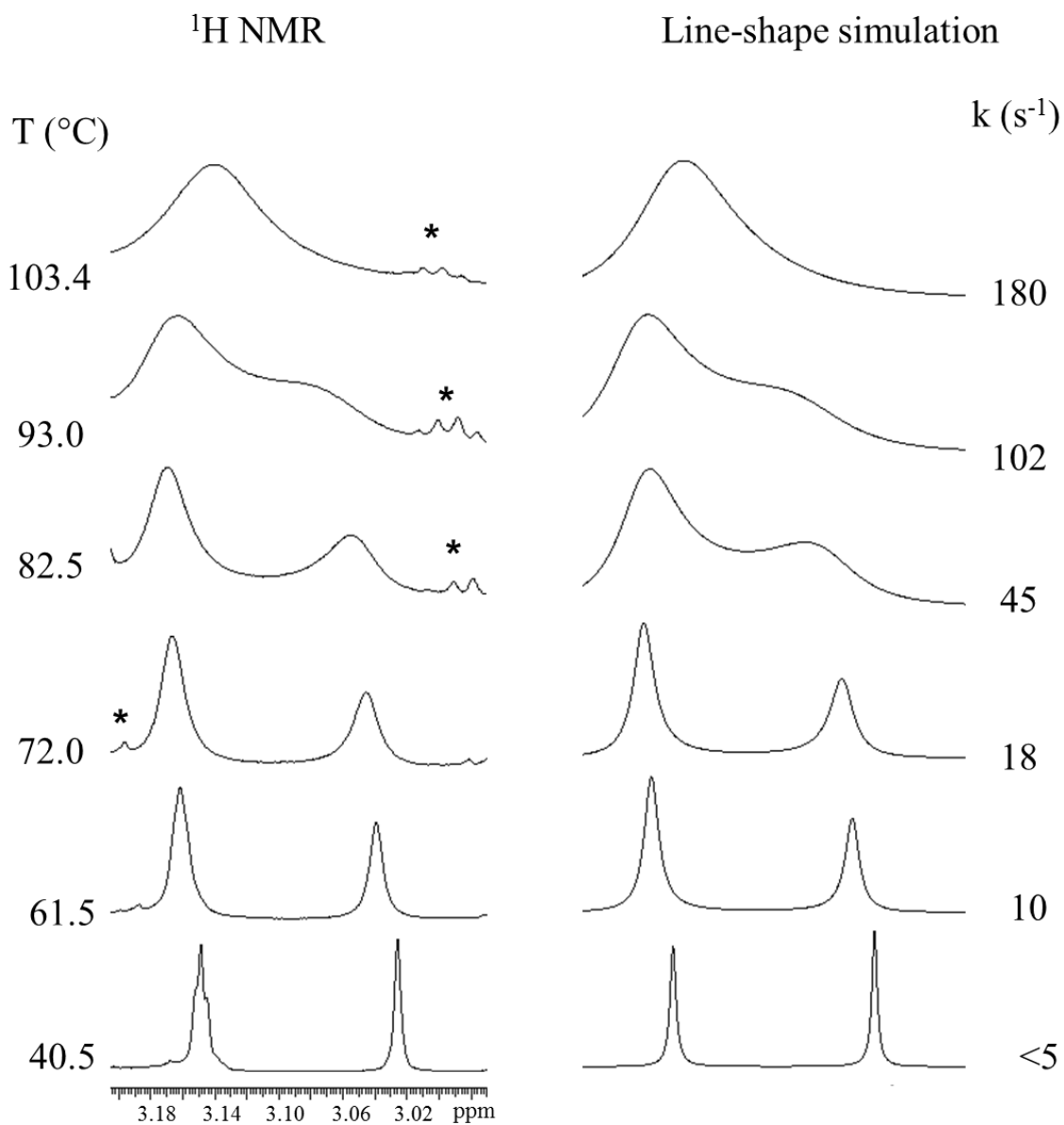
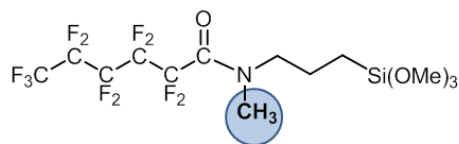
Basing on the optimization of the ground state geometries, a simplified structure of compound **2**, named **Et-2**, was taken into account. In this model compound, the three-methylene chain bearing the silane moiety was replaced with an ethyl group, reducing the number of conformations with unrelevant energy barriers to be considered [40]. After DFT minimization [41], only two stable conformations were obtained, with a calculated population distribution of almost 50:50 (Fig. 1).



**Fig. 1.** Calculated ground state and transition state for compound Et-2.

Ground state geometries show that the amide carbonyl group is coplanar with the trigonal planar *N* of the amide, being either on the same side of the methyl group (*E*-GS1) or on the opposite side (*Z*-GS; see Fig. 1). In the transition state, the trigonal *N* of the amide is distorted from planarity [42] with

a 116° angle (TS1) and 66° (TS2), with a calculated barrier of 19.07 kcal/mol and 20.25 kcal/mol respectively. The torsional barriers of the model compound were determined by line-shape analysis of NMR spectra recorded at variable temperature (Fig. 2). The NMR spectrum obtained at 40.5°C showed two distinct signals for the *N*-Me group, with 60:40 population distribution. Upon raising the temperature, the signals broadened and finally coalesced at 93°C. The experimental energy barrier, determined by line-shape simulation as (18.0±0.2) kcal/mol [43], is in good agreement with the calculated one.



**Fig. 2.** (Left) temperature dependence of the  $^1\text{H}$  N-Me signal of **2** (600 MHz in  $\text{C}_2\text{D}_2\text{Cl}_4$ ). (Right) Line-shape simulation, with the corresponding rate constants. Stars indicate peak impurities.

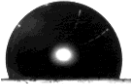

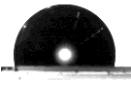

### 3.2. Characterization of ITO-FAS systems

The FAS **2** and **3** were chemically bound to the ITO surface, a substrate chosen for its conducting and transparent properties [22] and their performances were evaluated and compared with those of **1** and **4**.

Water CA measurement is one of the most sensitive probes to provide a measure of the interfacial hydrophobicity and oleophobicity of the examined FAS [44][45]. The static CAs for the target systems are reported in Table 1.

**Table 1**

Static CAs and Surface Free Energies<sup>a</sup>; EIS parameters for the target specimens.<sup>b</sup>

Sample	$\Theta_{\text{H}_2\text{O}}$ (°)	$\Theta_{\text{CH}_2\text{I}_2}$ (°)	$\gamma_1$ (mJ×m <sup>-2</sup> )	$\gamma_1^d$ (mJ×m <sup>-2</sup> )	$\gamma_1^p$ (mJ×m <sup>-2</sup> )	$R_{ct}$ ( $\Omega$ )	CPE ( $\mu\text{Fcm}^{-2}$ )
bare ITO <sup>c</sup>	81±6	43.6±1.6	41.0	37.8	3.2	305±5	12.4±0.1
<b>ITO-1</b> <sup>c</sup>	113.5±2.9	88 ±4	14.0	13.6	0.4	13000±600	1.9±0.1
<b>ITO-2</b>	111.0±0.7 	90.4±1.2 	13.4	12.5	0.9	-	-
<b>ITO-3</b>	106.1±1.2 	87.1±1.6 	15.6	14.1	1.5	293±8	10.7 ±0.3
<b>ITO-4</b> <sup>b</sup>	99±5	70±5	24.1	22.8	1.4	1013±52	3.3±0.2

<sup>a</sup> The liquid surface tension of water and diiodomethane used for the calculation are reported in Table S1.

<sup>b</sup> All the analysis were done on three replicas, and the relative uncertainty resulted within ± 5 %.

<sup>c</sup> Ref. 15.

As expected, an increase of the contact angle is observed when the ITO surface is modified with the fluoroalkylsilanes, due to the hydrophobic character of the latter. Nevertheless, whereas CAs in water for **ITO-1**-and **ITO-2** (both having a C<sub>5</sub>F<sub>11</sub> perfluorinated tail) are very close, a slightly lower value is obtained for **ITO-3** (R<sub>F</sub> = C<sub>3</sub>F<sub>7</sub>). In the case of **ITO-4** having a C<sub>6</sub>F<sub>13</sub> tail but *no* embedded amide

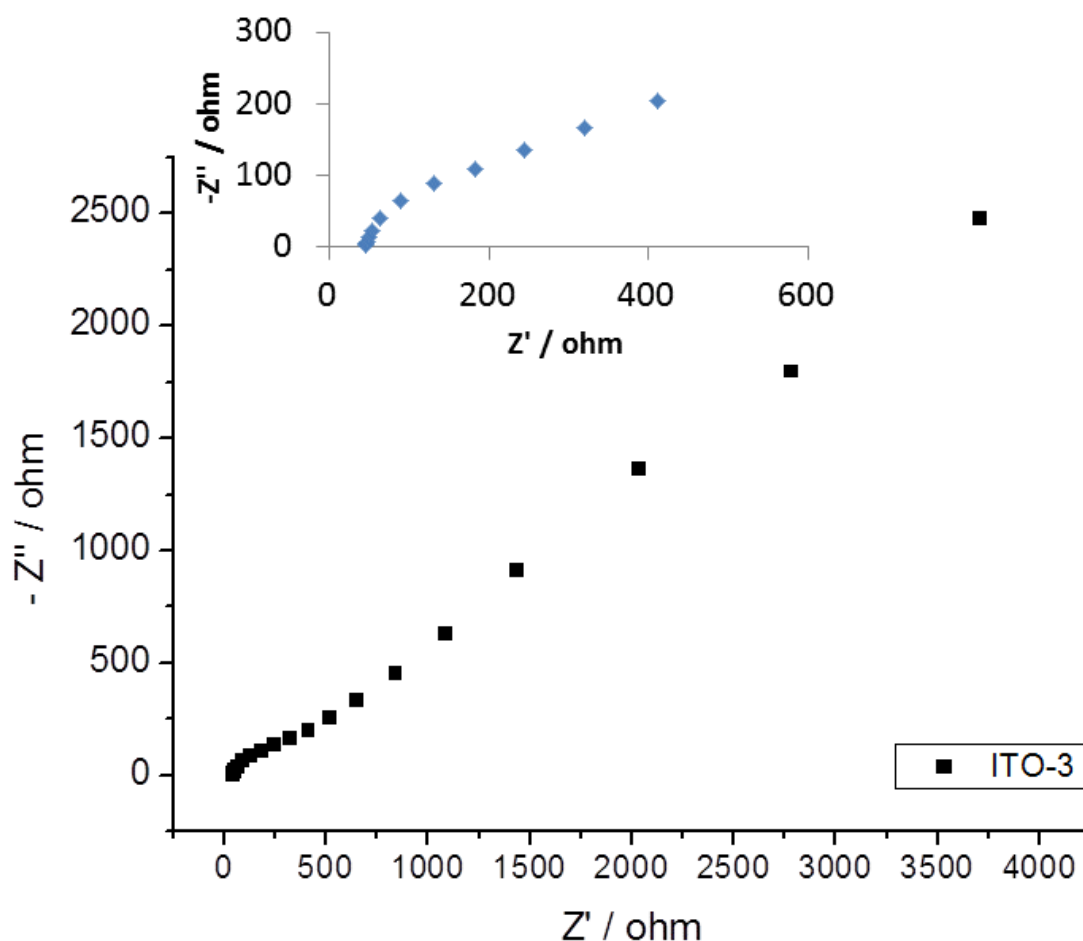
groups, the measured CA value is significantly lower. Similar conclusions can be drawn from the CAs data in diiodomethane shown in Table 1.

Surface free energies ( $\gamma$ ) with their disperse ( $\gamma^d$ ) and polar fractions ( $\gamma^p$ ) are also reported in Table 1 [31]. In agreement with the observed CAs values, a significant variation in these values took place for the FAS-modified surface, and similar  $\gamma$  values were obtained upon using **1**, **2** and **3**. The comparable values observed for **ITO-1** and **ITO-2**, possessing the same  $R_F$  length, suggest that the presence of the -N(CH<sub>3</sub>)CO- group instead of the -N(H)CO- one does not appreciably affect surface properties. Furthermore, the close values observed for **ITO-1** and **ITO-3** show that a decrease of two  $R_F$  units does not significantly impact the hydrophobicity of the modified ITO. Conversely, a completely different behavior was observed for **ITO-4**, whose  $\gamma$  is higher than 20 mJ×m<sup>-2</sup>, the value normally considered the upper limit for amphiphobic (*i.e.* oleophobic and hydrophobic) surfaces. It is worth reminding that the  $\gamma$  reported for poly(tetrafluoroethylene) (PTFE, Teflon) and CF<sub>3</sub>(CF<sub>2</sub>)<sub>7</sub>CH<sub>2</sub>CH<sub>2</sub>Si(OMe)<sub>3</sub> (often abbreviated as FAS17) correspond to 18.5 and 12 mJ×m<sup>-2</sup>, respectively [46][47][48][49].

EIS has been used to measure the ionic conductivity of the ITO-FAS systems; their charge transfer resistance was calculated measuring the diffusion of the redox probe K<sub>4</sub>[Fe(CN)<sub>6</sub>]/K<sub>3</sub>[Fe(CN)<sub>6</sub>] [50]. The higher the charge transfer resistance of the electroactive surface ( $R_{ct}$ , diameter of the semicircle portion of the Nyquist plot), the higher is the insulating character of the layer [51]. Table 1 reports the  $R_{ct}$  and CPE values [52][53][54].

As previously reported, the Nyquist plot of bare ITO presented a very small semicircle in the high frequency region and a straight line in the low-frequency one, indicating that the electron transfer process of the redox couple is essentially diffusion-controlled [15]. On the contrary, the presence of FAS **1** and **4** on the ITO surface resulted in a considerable semicircle enlargement, due to the increase in charge transfer resistance (*i.e.*, increase of the blocking behaviour of the self-assembled layers). The high  $R_{ct}$  value observed for **ITO-1** was attributed to the ability of the internal -N(H)CO- moiety

to generate hydrogen bonds between neighbouring molecules and to create an ordered layer endowed with good insulating proprieties [16]17][55][56]. **ITO-3** ( $R_F = C_3F_7$ ) showed a  $R_{ct}$  similar to that of bare ITO (Table 1, Fig. 3), suggesting the occurrence of an easier electronic transport. This result suggests that amide groups, in the presence of a short capping perfluorinated chain, are unable to affect the rate of electron transfer across the layer. In contrast to the ITO-FAS examined so far, **ITO-2** presented a poor reproducibility of the  $R_{ct}$  and CPE values. This behaviour was attributed to the co-presence of two *E/Z* conformations (see above) that, during ITO functionalization, give rise to a disordered packing of the target molecules.



**Fig. 3.** Nyquist plots for **ITO-3**.

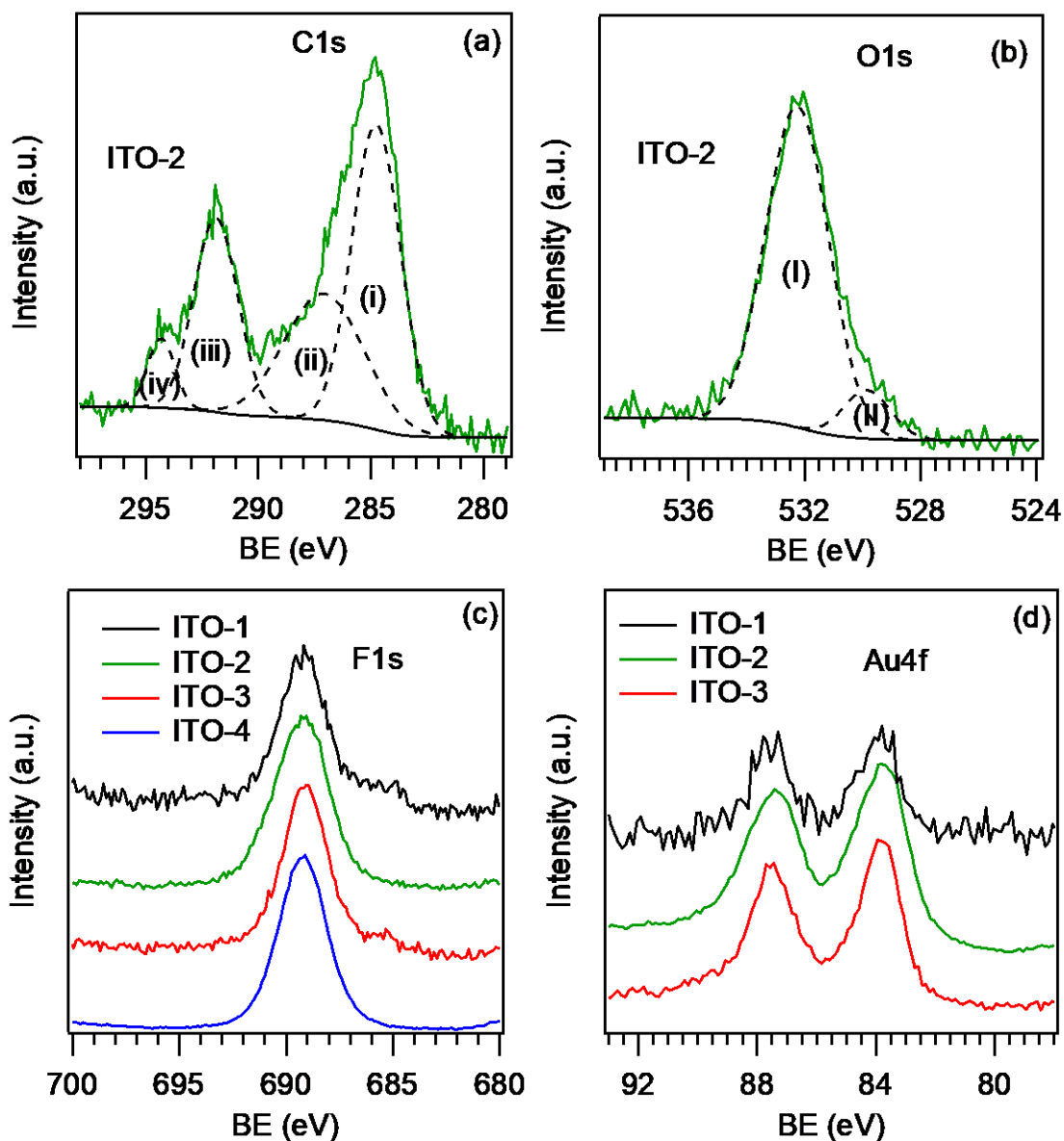
### 3.2. Characterization of AuNPs/ITO-FAS systems

The chemical composition of AuNPs/ITO-FAS systems was investigated by XPS. Regardless of the preparative conditions, survey spectra (Fig. S1) revealed the main presence of C, O, F, Sn and In, whose presence was related to the polymeric chain and to the used substrate. Irrespective of the preparative conditions, the C1s signal could be deconvoluted by means of four components (see Fig. 4a as a representative example): (i), BE = 284.8 eV, assigned both to adventitious carbon contaminations and to C-C bonds from the used matrices; (ii), BE = 286.9 eV, attributed to C-O bonds; (iii), BE = 291.8 eV and (iv), BE = 294.0 eV, ascribed to CF<sub>x</sub> moieties in the perfluorinated tails [57][58]. For all the analysed specimens, two peaks contributed to the O1s signal (Fig. 2b): (I), BE = 532.6 eV, ascribed to oxygen species in the organosilane; (II), BE = 530.0 eV, due to lattice O in ITO (substrate) [57][59][60].

As a general observation, the F1s peak, centred at BE  $\approx$  689.0 eV (Fig. 4c), resulted from fluorine presence in CF<sub>x</sub> groups [57][61]. Apart for **ITO-4** (in which the Au signal was below the detection limits), for all the other specimens the Au4f peak (Fig. 4d) displayed two spin-orbit components and the position of the Au4f<sub>7/2</sub> [BE = 83.8 eV] confirmed the metallic state of Au nanoparticles [57][59][63]. Interestingly, the samples were characterized by different surface atomic concentration of Au, clearly highlighting the role of the polymeric chain. In particular, Au surface atomic percentages were calculated to be: **ITO-1**: 0.3 at.%; **ITO-2**: 5.5 at.%; **ITO-3**: 2.0 at.%. In addition, it is worthwhile noting that: i) the Au at.% is related to the number of Au NPs (Fig. S4); ii) since each silane molecule has only one Si atoms, the Si at.% can be associated to the number of silane molecules. On this basis, the ratio between Au at.% and Si at.% concentration can yield information on the Au NPs concentration as a function of the number of silane molecules. The obtained (Au at.)/(Si at. %) data highlight a higher Au NP content in the **ITO-2** specimen, in line with the SEM data analysis (**ITO-1**: 0.05; **ITO-2**: 0.80; **ITO-3**: 0.65, see below).

The analysis of N1s signals (Fig. S2) revealed similar features for **ITO-1**, **ITO-2** and **ITO-3** samples (excluding sample **ITO-4** in which N was not present), and the band centered at BE = 400.3

eV could be attributed to  $-N(R)C1O-$  groups [57][59][63]. Interestingly, the N concentration (**ITO-1**: 0.5 at.%; **ITO-2**: 3.2 at.%; **ITO-3**: 2.5 at.%) displayed the same trend as the Au at.%, highlighting the role on N species in the immobilization of AuNPs [64][65]. This conclusion was further supported by the absence of Au signal in the sample **ITO-4**, in which N-groups were not present.

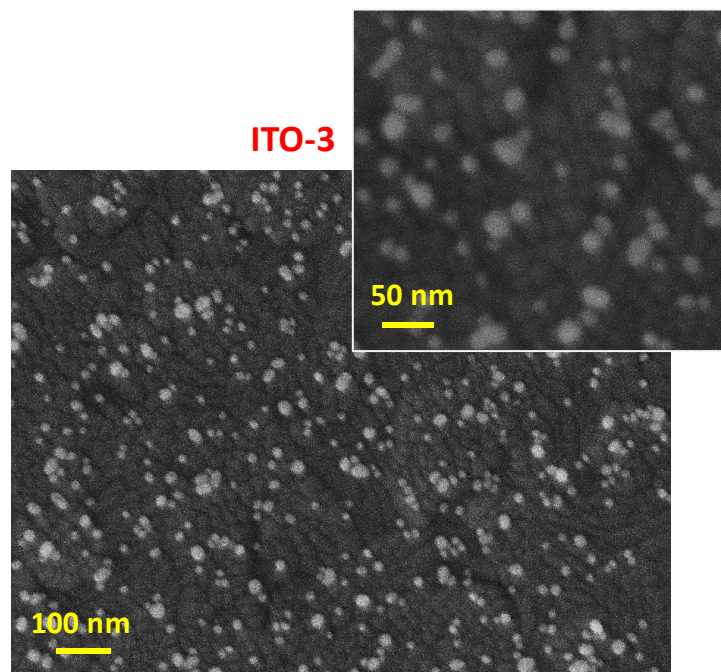
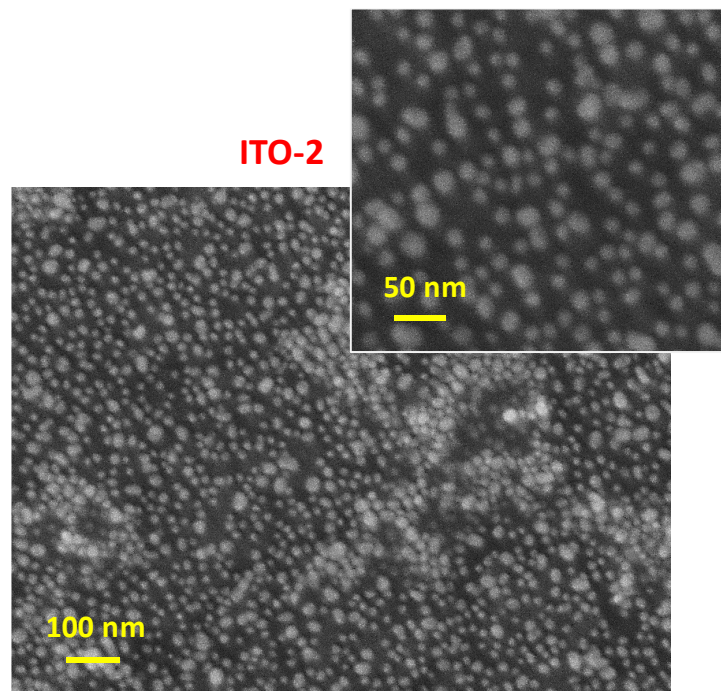


**Fig. 4.** Surface XPS signals: (a) C1s and (b) O1s peaks for a representative sample (**ITO-2**); (c) F1s signals for all the analysed specimens; (d) Au4f peaks for all Au-containing samples (**ITO-1**, **ITO-2** and **ITO-3**).

In order to obtain a further confirmation regarding the important role played by the amide nitrogen towards AuNPs distribution, a detailed FE-SEM investigation was performed as a function of

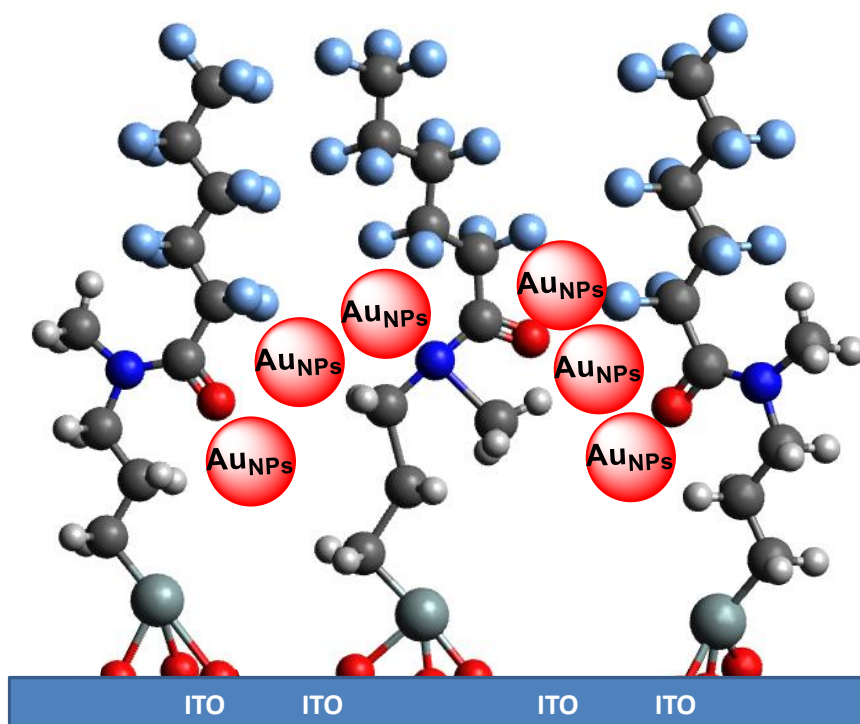


the adopted processing conditions. For all the target systems, the analyses confirm the presence of AuNPs characterized by an average size of  $(15 \pm 4)$  nm (see Fig. 5 and Fig. S3), a value very close to the one of the pristine colloidal solution. Nevertheless, the recorded FE-SEM images (see Fig. 5 and Fig. S3) enabled to confirm that the dispersion of the AuNPs was appreciably influenced by the chemical nature of the used FAS molecules, giving rise to a different NP surface coverage (SC %) with the following trend: 60% **ITO-2** > 16% **ITO-3** > 9% **ITO-1** > 3% **ITO-4**.



**Fig. 5.** Representative FE-SEM micrographs pertaining to the samples **ITO-2** and **ITO-3** collected at different magnification levels.

The highest value of SC% was obtained for the sample characterized by the presence of a methyl group on the amide nitrogen, which may result, as reported in Scheme 2 and in agreement with EIS data discussed in the previous section, in the formation of a less compact and more disordered FAS layer enabling an easier penetration of AuNPs within the hosting material [58].



**Scheme 2.** Schematic representation for the **AuNPs/ITO-2** system.

These evidences agree to a good extent with the above reported XPS results for surface Au at% of each sample and are further corroborated by the linear trend obtained by plotting the XPS surface Au at% *versus* the extrapolated Au SC% values (see Fig. S4). This result is indeed of great importance for the possibility of controlling the gold loading on electroactive surfaces modified by a silane-based fluorinated coating.

## Conclusions

In this work we studied the influence that an embedded amide functional group  $-N(R)CO-$  ( $R = H, CH_3$ ) has on the structure and surface properties of ITO silanized with FAS having formula  $R_F C(O)N(R)(CH_2)_3 Si(OMe)_3$  (**1**,  $R = H, R_F = C_5F_{11}$ ; **2**,  $R = CH_3, R_F = C_5F_{11}$ ; **3**,  $R = H, R_F = C_3F_7$ ). The results were compared with what found with  $R_F(CH_2)_2 Si(OEt)_3$  (**4**,  $R_F = C_6F_{13}$ ) and significant differences were observed.

We found that the systems **ITO-1**, **ITO-2** and **ITO-3** show comparable surface properties: the CAs in water are very similar ( $113.5^\circ, 111.0^\circ, 106.1^\circ$ ) and higher than **ITO-4** ( $99.2^\circ$ ) confirming that the amide group can efficiently balance the lower fluorine content in the surface hydrophobization of materials. Indeed also similar surface free energies were found for the former class of samples that present an amphiphobic nature.

On the other hand the EIS electrochemical characterization of ITO-FAS coupled with the XPS and FE-SEM characterization of  $Au_{NPs}/ITO-FAS$  has allowed to shed light on the chemical-physical changes occurring on the modified ITO when i) the amide nitrogen is bearing a proton or a methyl or ii) the length of the perfluorinated tail is shorten of two units from  $C_5F_{11}$  to  $C_3F_7$ . The behaviour of the organosilane  $C_5F_{11}C(O)N(CH_3)(CH_2)_3 Si(OMe)_3$  (**2**) is particularly noteworthy. VT NMR studies revealed that the presence of a methyl group on the amide nitrogen increase the steric hindrance in the rotation around the  $N-CO$  bond generating, at room temperature, two stable *E* and *Z* conformations with a 60:40 population ratio. The presence of these two conformers in solution combined with the lack of intermolecular  $N-H \cdots OC-N$  hydrogen bond among the anchored molecules, has dramatic influences on the silanized ITO giving rise to a disordererly packed coating layer able to accommodate a large quantity of  $Au_{NPs}$ .

These results indicated that  $Au_{NPs}$  can have a dual role: i) they can act as excellent probe to evaluate the morphology of the coating layer; ii) their degree of immobilization on electroactive surfaces modified by different silane-based fluorinated coatings can be tuned depending on the silane structure.

## Appendix A. Supplementary data

Supplementary data associated with this article can be found in the online version, at <http://.....>

## Acknowledgments

The authors B.B., M.C.C. and D.N. thank the University of Bologna for financial support. The authors D.B., C.M., G.C. acknowledge financial support under Padova University ex-60% 2014–2017, PDiSC #SENSATIONAL BIRD2016-UNIPD project and ACTION post-doc fellowship.

## References

- [1] B. Ameduri, B. Boutevin, *Well-Architected Fluoropolymers: Synthesis, Properties and Applications* 1st Edition, Elsevier, London, 2004.
- [2] S. Banerjee, D.D. Dionysiou, S.C. Pillai, Self-cleaning applications of TiO<sub>2</sub> by photo-induced hydrophilicity and photocatalysis, *Appl. Catal. B Environ.* 176–177 (2015) 396–428.
- [3] J.D. Brassard, D.K. Sarkar, J. Perron, Synthesis of monodisperse fluorinated silica nanoparticles and their superhydrophobic thin films, *ACS Appl. Mater. Interfaces.* 3 (2011) 3583–3588.
- [4] M. Lejars, A. Margailan, C. Bressy, Fouling release coatings: A non toxic alternative to biocidal antifouling coatings, *Chem. Rev.* 112 (2012) 4347–4390.
- [5] S. Wang, K. Liu, X. Yao, L. Jiang, Bioinspired surfaces with superwettability: New insight on theory, design, and applications, *Chem. Rev.* 115 (2015) 8230–8293.
- [6] J.-M. Vincent, Recent advances of fluoruous chemistry in material sciences, *Chem. Commun.* 48 (2012) 11382–11391.
- [7] M. Pagliaro, C. R., New fluorinated functional materials, *J. Mater. Chem.* 15 (2005) 4981–4991.

- [8] M.P. Krafft, J.G. Riess, Selected physicochemical aspects of poly- and perfluoroalkylated substances relevant to performance, environment and sustainability-Part one, *Chemosphere*. 129 (2015) 4–19.
- [9] M.P. Krafft, J.G. Riess, Per- and polyfluorinated substances (PFASs): Environmental challenges, *Curr. Opin. Colloid Interface Sci.* 20 (2015) 192–212.
- [10] S. Valsecchi, M. Rusconi, S. Polesello, Determination of perfluorinated compounds in aquatic organisms: A review, *Anal. Bioanal. Chem.* 405 (2013) 143–157.
- [11] K. Saha, S.S. Agasti, C. Kim, X. Li, V.M. Rotello, Gold nanoparticles in chemical and biological sensing, *Chem. Rev.* 112 (2012) 2739–2779.
- [12] E. Priyadarshini, N. Pradhan, Gold nanoparticles as efficient sensors in colorimetric detection of toxic metal ions: A review, *Sensors Actuators, B Chem.* 238 (2017) 888–902.
- [13] E.A. de Oliveira Farias, S.S. Nogueira, A.M. de Oliveira Farias, M.S. de Oliveira, M. de Fátima Cardoso Soares, H.N. da Cunha, J.R. Dos Santos Junior, D.A. da Silva, P. Eaton, C. Eiras, A thin PANI and carrageenan–gold nanoparticle film on a flexible gold electrode as a conductive and low-cost platform for sensing in a physiological environment, *J. Mater. Sci.* (2017) 1–13.
- [14] S. Kinge, M. Crego-Calama, D.N. Reinhoudt, Self-assembling nanoparticles at surfaces and interfaces, *ChemPhysChem.* 9 (2008) 20–42.
- [15] B. Ballarin, D. Barreca, M.C. Cassani, G. Carraro, C. Maccato, A. Mignani, D. Lazzari, M. Bertola, Fluoroalkylsilanes with Embedded Functional Groups as Building Blocks for Environmentally Safer Self-Assembled Monolayers, *Langmuir.* 31 (2015) 6988–6994.
- [16] R.S. Clegg, J.E. Hutchison, Molecular Films for Study of Through-Peptide Electron Transfer, *Langmuir.* 12 (1996) 5239–5243.
- [17] S.W. Tarn-Chang, H.A. Biebuyck, G.M. Whitesides, N. Jeon, R.G. Nuzzo, Self-Assembled Monolayers on Gold Generated from Alkanethiols with the Structure RNHCOCH<sub>2</sub>SH, *Langmuir.* 11 (1995) 4371–4382.

- [18] B. Ballarin, D. Barreca, M.C. Cassani, G. Carraro, C. Maccato, A. Mignani, D. Lazzari, M. Bertola, Gold nanoparticles-decorated fluoroalkylsilane nano-assemblies for electrocatalytic applications, *Appl. Surf. Sci.* 362 (2016) 42–48.
- [19] Miteni S.p.A. (<http://www.miteni.com>) is part of I.C.I.G. (International Chemical Investors Group, <http://www.ic-investors.com/>) an industrial group operating worldwide in base chemicals, fine chemicals, and polymers.
- [20] J.H. Simons, *Fluorine Chemistry*, Vol. 1, Academic Press, New York, 1950.
- [21] F.G. Drakesmith, Electrofluorination of Organic Compounds. In: Chambers R.D. (eds) *Organofluorine Chemistry. Topics in Current Chemistry*, Vol. 193, Springer, Berlin, Heidelberg, 1997.
- [22] B. Ballarin, M.C. Cassani, E. Scavetta, D. Tonelli, Self-assembled gold nanoparticles modified ITO electrodes: The monolayer binder molecule effect, *Electrochim. Acta.* 53 (2008) 8034–8044.
- [23] J. Zhang, M. Oyama, Gold nanoparticle-attached ITO as a biocompatible matrix for myoglobin immobilization: Direct electrochemistry and catalysis to hydrogen peroxide, *J. Electroanal. Chem.* 577 (2005) 273–279.
- [24] The AuNPs colloidal solution was obtained by reduction of aqueous HAuCl<sub>4</sub> with trisodium citrate (pH 6.0, 1.1 mM).
- [25] P.J. Stephens, F.J. Devlin, C.F. Chabalowski, M.J. Frisch, Ab Initio Calculation of Vibrational Absorption and Circular Dichroism Spectra Using Density Functional Force Fields, *J. Phys. Chem.* 98 (1994) 11623–11627.
- [26] M.J.. Frisch, G.W. Trucks, H.B. Schlegel, G.E. Scuseria, M.A. Robb, G. Cheeseman, J. R. Scalmani, V. Barone, B. Mennucci, G.A. Petersson, H. Nakatsuji, M. Caricato, X. Li, H.P. Hratchian, A.F. Izmaylov, J. Bloino, G. Zheng, J.L. Sonnenberg, M. Hada, M. Ehara, K. Toyota, R. Fukuda, J. Hasegawa, M. Ishida, T. Nakajima, Y. Honda, O. Kitao, H. Nakai, T. Vreven, J. Montgomery, J. A., J.E. Peralta, F. Ogliaro, M. Bearpark, J.J. Heyd, E. Brothers,

- K.N. Kudin, V.N. Staroverov, R. Kobayashi, J. Normand, K. Raghavachari, A. Rendell, J.C. Burant, S.S. Iyengar, J. Tomasi, M. Cossi, N. Rega, N.J. Millam, M. Klene, J.E. Knox, J.B. Cross, V. Bakken, C. Adamo, J. Jaramillo, R. Gomperts, R.E. Stratmann, O. Yazyev, A.J. Austin, R. Cammi, C. Pomelli, J.W. Ochterski, R.L. Martin, K. Morokuma, V.G. Zakrzewski, G.A. Voth, P. Salvador, J.J. Dannenberg, S. Dapprich, A.D. Daniels, O. Farkas, J.B. Foresman, J. V. Ortiz, J. Cioslowski, D.J. Fox, Gaussian 09, rev D.01, (2009).
- [27] P.Y. Ayala, H.B. Schlegel, Identification and treatment of internal rotation in normal mode vibrational analysis, *J. Chem. Phys.* 108 (1998) 2314–2325.
- [28] C.F. Tormena, R. Rittner, R.J. Abraham, E.A. Basso, B.C. Fiorin, Conformational analysis of fluoroacetoxime and of its O-methyl ether by  $^1\text{H}$ ,  $^{13}\text{C}$  and  $^{15}\text{N}$  NMR and theoretical calculations, *J. Phys. Org. Chem.* 17 (2004) 42–48.
- [29] S.E. Wheeler, A.J. Mcneil, P. Mu, T.M. Swager, Probing Substituent Effects in Aryl - Aryl Interactions Using Stereoselective Diels - Alder Cycloadditions, 26 (2010) 3304–3311.
- [30] D. Briggs, M.P. Seah, *Practical Surface Analysis: Vol. 1, Auger and X-ray Photoelectron Spectroscopy*, Wiley, New York, 1990.
- [31] A. Rudawska, E. Jacniacka, Analysis for determining surface free energy uncertainty by the Owen–Wendt method, *Int. J. Adhes. Adhes.* 29 (2009) 451–457.
- [32] H.S. Gutowsky, C.H. Holm, Rate Processes and Nuclear Magnetic Resonance Spectra. II. Hindered Internal Rotation of Amides, *J. Chem. Phys.* 25 (1956) 1228–1234.
- [33] R.F. Hobson, L.W. Reeves, R.C. Shaddick, Hindered rotation about the amido N-C bond and the tautomeric equilibrium in N,N-dimethylacetoacetamide, *Org. Magn. Reson.* 6 (1974) 129–132.
- [34] M. Feigel, Rotation barriers of amides in the gas phase, *J. Phys. Chem.* 87 (1983) 3054–3058.
- [35] A. Mazzanti, M. Chiarucci, L. Prati, K.W. Bentley, C. Wolf, Computational and DNMR Analysis of the Conformational Isomers and Stereodynamics of Secondary 2,2'-Bisanilides,

- J. Org. Chem. 81 (2016) 89–99.
- [36] J. Sandoval-Lira, L. Fuentes, L. Quintero, H. Höpfl, J.M. Hernández-Pérez, J.L. Terán, F. Sartillo-Piscil, The stabilizing role of the intramolecular C-H···O hydrogen bond in cyclic amides derived from  $\alpha$ -methylbenzylamine, J. Org. Chem. 80 (2015) 4481–4490.
- [37] L.W. Reeves, R.C. Shaddick, K.N. Shaw, Nuclear Magnetic Resonance Studies of Multi-site Chemical Exchange. 111. Hindered Rotation in Dimethylacetamide, Dimethyl Trifluoroacetamide, and Dimethyl Benzamide, Can. J. Chem. 49 (1971) 3683–3692.
- [38] C.L. LeMaster, C.B. LeMaster, N.S. True, Gas-phase nuclear magnetic resonance study of ( $^{15}\text{N}$ )trifluoroacetamide: Comparison of experimental and computed kinetic parameters, J. Am. Chem. Soc. 121 (1999) 4478–4484.
- [39] C. Suarez, E.J. Nicholas, M.R. Bowman, Gas-phase dynamic NMR study of the internal rotation in N-trifluoroacetylpyrrolidine, J.Phys.Chem.A. 107 (2003) 3024–3029.
- [40] P.L. Polavarapu, E.A. Donahue, G. Shanmugam, G. Scalmani, E.K. Hawkins, C. Rizzo, I. Ibnusaud, G. Thomas, D. Habel, D. Sebastian, A single chiroptical spectroscopic method may not be able to establish the absolute configurations of diastereomers: Dimethylesters of hibiscus and garcinia acids, J. Phys. Chem. A. 115 (2011) 5665–5673.
- [41] All the conformations found by MM search within a 10 kcal/mol window (Monte Carlo searching together with the MMFF94 molecular mechanics force field as implemented in Titan 1.0.5, Wavefunction inc.) were then optimized using DFT at the B3LYP/6-31G(d) level.
- [42] Y. Jean, I. Demachy, A. Lledos, F. Maseras, Electronic against steric effects in distorted amides, J. Mol. Struct. THEOCHEM. 632 (2003) 131–144.
- [43] The indicated error refer to the absolute errors due to the uncertainty in the temperature determination.
- [44] C. Ruan, T. Bayer, S. Meth, C.N. Sukenik, Creation and characterization of n -alkylthiol and n -alkylamine self-assembled monolayers on 316L stainless steel, Thin Solid Films. 419



(2002) 95–104.

- [45] B. Choplin, F.; Navarre, S.; Bousbaa, J.; Babin, P.; Bennetau, B.; Bruneel, J. L.; Desbat, Structural Characterization of Self-Assembled Monolayers by Unenhanced Raman Spectroscopy, *J. Raman Spectrosc.* 34 (2003) 902–906.
- [46] K.L. Mittal, ed., *Silanes and Other Coupling Agents*, Vol. 5, CRC Press, Boca Raton, FL, 2009.
- [47] A.S.H. Makhlof, ed., *Handbook of Smart Coatings for Materials Protection*, 1st ed., Woodhead Publishing (Elsevier), 2014.
- [48] H.-J. Butt, C. Semprebon, P. Papadopoulos, D. Vollmer, M. Brinkmann, M. Ciccotti, Design principles for superamphiphobic surfaces, *Soft Matter*. 9 (2013) 418–428.
- [49] M. Hikita, K. Tanaka, T. Nakamura, T. Kajiyama, A. Takahara, Super-liquid-repellent surfaces prepared by colloidal silica nanoparticles covered with fluoroalkyl groups, *Langmuir*. 21 (2005) 7299–7302.
- [50] W. Knoll, R.C. Advincula, eds., *Functional Polymer Films. Volume 2: Characterization and Applications*, Wiley-VCH, 2011.
- [51] Y. Wei, L.-T. Kong, R. Yang, L. Wang, J.-H. Liu, X.-J. Huang, Electrochemical impedance determination of polychlorinated biphenyl using a pyrenecyclodextrin-decorated single-walled carbon nanotube hybrid., *Chem. Commun. (Camb)*. 47 (2011) 5340–2.
- [52] The CPE represents a circuit parameter with limiting behavior as a capacitor for  $n = 1$  or a resistor for  $n = 0$ , where  $n$  is the exponent in the a CPE's impedance mathematical formula [53]; in our case  $n$  is always very close to 1 ( $0.997 \pm 0.001$ ) [51].
- [53] J.B. Jorcin, M.E. Orazem, N. Pébère, B. Tribollet, CPE analysis by local electrochemical impedance spectroscopy, *Electrochim. Acta*. 51 (2006) 1473–1479.
- [54] J.R. Macdonald, W.R. Kenan, *Impedance Spectroscopy: Emphasizing Solid Materials and Analysis*, Wiley, New York, 1987.
- [55] S. Sek, B. Palys, R. Bilewicz, Contribution of intermolecular interactions to electron transfer

- through monolayers of alkanethiols containing amide groups, *J. Phys. Chem. B.* 106 (2002) 5907–5914.
- [56] R.S. Clegg, S.M. Reed, R.K. Smith, B.L. Barron, J.A. Rear, J.E. Hutchison, Interplay of lateral and tiered interactions in stratified self-organized molecular assemblies, *Langmuir.* 15 (1999) 8876–8883.
- [57] J.F. Moulder, W.F. Stickle, P.E. Sobol, K.D. Bomben, *Handbook of X-ray Photoelectron Spectroscopy*, (1992) 261. [58] J. Zuo, P. Keil, M. Valtiner, P. Thissen, G. Grundmeier, Deposition of Ag nanoparticles on fluoroalkylsilane self-assembled monolayers with varying chain length, *Surf. Sci.* 602 (2008) 3750–3759.
- [59] <http://srdata.nist.gov/xps/>
- [60] A. Chen, K. Zhu, H. Zhong, Q. Shao, G. Ge, A new investigation of oxygen flow influence on ITO thin films by magnetron sputtering, *Sol. Energy Mater. Sol. Cells.* 120 (2014) 157–162.
- [61] C. Zhang, Y. Chen, Investigation of fluorinated polyacrylate latex with core-shell structure, *Polym. Int.* 54 (2005) 1027–1033.
- [62] L. Armelao, D. Barreca, G. Bottaro, A. Bovo, A. Gasparotto, E. Tondello, Characterization of Au/TiO<sub>2</sub> Nanocomposites by XPS, *Surf. Sci. Spectra.* 10 (2003) 1–7.
- [63] G. Billon, B. Ouddane, L. Gengembre, A. Boughriet, On the Chemical Properties of Sedimentary Sulfur in Estuarine Environments, *Phys. Chem. Chem. Phys.* 4 (2002) 751–756.
- [64] M. Giorgetti, G. Aquilanti, B. Ballarin, M. Berrettoni, M.C. Cassani, S. Fazzini, D. Nanni, D. Tonelli, Speciation of gold nanoparticles by Ex situ extended X-ray absorption fine structure and X-ray absorption near edge structure, *Anal. Chem.* 88 (2016) 6873–6880.
- [65] S. Fazzini, D. Nanni, B. Ballarin, M.C. Cassani, M. Giorgetti, C. MacCato, A. Trapananti, G. Aquilanti, S.I. Ahmed, Straightforward synthesis of gold nanoparticles supported on commercial silica-polyethyleneimine beads, *J. Phys. Chem. C.* 116 (2012) 25434–25443.